PNAS RESEARCH ARTICLE | NEUROSCIENCE

Comparing human and chimpanzee temporal lobe neuroanatomy reveals modifications to human language hubs beyond the frontotemporal arcuate fasciculus

Joanna Sierpowska[a,b,2,1], Katherine L. Bryant[a,c,1], Nikki Janssen[a,b,d], Guilherme Blazquez Freches[a,e], Manon Römkens[a,f], Margot Mangnus[a], Rogier B. Mars[a,c], and Vitoria Piai[a,b]

Edited by Marcus Raichle, Washington University in St. Louis, St. Louis, MO; received October 7, 2021; accepted May 11, 2022

The biological foundation for the language-ready brain in the human lineage remains a debated subject. In humans, the arcuate fasciculus (AF) white matter and the posterior portions of the middle temporal gyrus are crucial for language. Compared with other primates, the human AF has been shown to dramatically extend into the posterior temporal lobe, which forms the basis of a number of models of the structural connectivity basis of language. Recent advances in both language research and comparative neuroimaging invite a reassessment of the anatomical differences in language streams between humans and our closest relatives. Here, we show that posterior temporal connectivity via the AF in humans compared with chimpanzees is expanded in terms of its connectivity not just to the ventral frontal cortex but also to the parietal cortex. At the same time, posterior temporal regions connect more strongly to the ventral white matter in chimpanzees as opposed to humans. This pattern is present in both brain hemispheres. Additionally, we show that the anterior temporal lobe harbors a combination of connections present in both species through the inferior fronto-occipital fascicle and human-unique expansions through the uncinate and middle and inferior longitudinal fascicles. These findings elucidate structural changes that are unique to humans and may underlie the anatomical foundations for full-fledged language capacity.

white matter | language | evolution | arcuate fasciculus | temporal lobe

Significance

Communication through language is a great achievement of evolution. In humans, the arcuate fasciculus, white matter that extended dramatically during evolution, is known to subserve language. We investigated whether connections through critical language centers in the temporal lobe are uniquely human. We show that connectivity in the posterior temporal lobe via the arcuate fasciculus expanded bilaterally to frontal and parietal cortices in humans compared with chimpanzees. Concomitantly, the ventral tracts connect more strongly to posterior temporal regions in the chimpanzees than in humans. In the anterior temporal lobe, connections shared between both species and uniquely human expansions are present. Changes to human language streams extend beyond the arcuate fasciculus, including a suite of expansions to connectivity within the temporal lobes.

The discovery that the arcuate fasciculus (AF) and to a lesser extent, the superior longitudinal fascicle, are dramatically extended in the human brain compared with those of other primates provided crucial insight into the unique combination of anatomical features that may have laid the foundation for full-fledged language in the human lineage (1–3). This discovery spearheaded a major interest in species differences in the organization of temporal and prefrontal connectivity, two territories that are crucial for language in humans (e.g., refs. 4 and 5).

Along with this original evolutionary discovery, our understanding of the anatomical basis of language has advanced substantially. In particular, there is greater appreciation of the distinct roles of the anterior and posterior temporal lobes (6), increased focus on the bilateral processing of language (7, 8), improved understanding of the contributions of the ventral language pathway (9), and the development of a model for the relationship of dorsal and ventral pathways for human language (10). Regarding the anatomical organization of the AF, the original characterization of the tract as a single pathway (e.g., ref. 11; reviewed in ref. 12) has been refined by the identification of a more complex division of, for example, separate temporal–parietal, temporal–frontal, and parietal–frontal pathways (13). In sum, a new perspective of language processing in the human brain has emerged (14), impacting a greater network than previously assumed.

In parallel to the developments in our understanding of the anatomical basis of language, comparative neuroimaging has also advanced. High-quality neuroimaging data from nonhuman primates, including great apes, have become increasingly available (15, 16), accompanied by new techniques to quantify differences in brain organization across species (17, 18). Together, this progress allows for a much richer cross-species comparison with the human brain (4, 19), resulting, for example, in the publication of the first whole-brain white-matter atlases of the macaque monkey (20) and chimpanzee (21). Such results not only demonstrate a much more complex organization of cortical anatomy across species (22), but they also highlight the phylogenetic origins of presumed human adaptations for language (23). These recent findings can now be integrated with an increased appreciation of the behavioral abilities of great apes, including sophisticated organization of vocal output (24).

Author contributions: J.S., K.L.B., R.B.M., and V.P. designed research; K.L.B. and N.J. performed research; J.S., K.L.B., and G.B.F. contributed new reagents/analytic tools; J.S., K.L.B., N.J., G.B.F., M.R., M.M., and V.P. analyzed data; J.S., K.L.B., N.J., M.M., R.B.M., and V.P. wrote the paper; and G.B.F. and M.R. critically reviewed the manuscript.

The authors declare no competing interest.

This article is a PNAS Direct Submission.

[1]J.S. and K.L.B. contributed equally to this work.

[2]To whom correspondence may be addressed. Email: joanna.sierpowska@donders.ru.nl.

This article contains supporting information online at http://www.pnas.org/lookup/suppl/doi:10.1073/pnas.2118295119/-/DCSupplemental.

Published July 5, 2022.

Altogether, these parallel developments call for a reassessment of the anatomical differences in language streams between humans and our closest animal relative, the great ape. Until recently, the vast majority of comparative, language-related neuroanatomy works were focused on frontal lobe structural changes, especially within inferior frontal regions (e.g., refs. 25 and 26), disregarding other areas crucial for human language. Yet, new evidence suggests that there are important differences in the connectivity of temporal association areas between humans, chimpanzees, and other primates (27, 28). Here, we bring temporal brain areas into the picture by examining modifications in two major language-related hubs: the posterior middle temporal gyrus (pMTG) and the anterior temporal lobe (ATL). These two hubs have been postulated as crucial for understanding, using, and learning language, with detrimental consequences following from their damage or dysfunction. In humans, the pMTG is involved in assigning meaning to words (29, 30) and in syntax processing (31–33), whereas the ATL is involved in the formation of semantic representations (34, 35). Structurally, the human pMTG is the cortical termination of an extensive number of white-matter pathways from both dorsal and ventral language streams (36). By contrast, the ATL receives white-matter terminations predominantly from the ventral stream (9, 37).

Given the critical functional importance of these two hubs for language, in the present study we examined their connectivity in both hemispheres in relation to the organization of ventral and dorsal language pathways in both humans and chimpanzees. In doing so, we reconstructed all major white-matter tracts of the dorsal and ventral pathways in both species, including the AF "tripartite" subdivisions (frontotemporal, frontoparietal, and parietotemporal), using a large dataset of 29 high-resolution diffusion-weighted imaging (DWI) chimpanzee scans. Our results demonstrate modifications to pMTG and ATL connectivity in humans suggesting that evolutionary modifications to the language network encompass not only the AF but also include a complex suite of expansions to the connectivity of ventral and dorsal language pathways within the temporal lobe.

Results

Tractography from ATL and pMTG. By using probabilistic tractography from high-resolution diffusion-weighted images of 50 humans and 29 chimpanzees, we generated tractograms originating from two seeds in each hemisphere, the ATL and the pMTG. The tractograms from the left ATL seed revealed an extensive ventral system of white-matter pathways (including a well-defined inferior fronto-occipital fascicle) in both humans and chimpanzees (Fig. 1). The tractograms did not substantially differ between the two species, reaching the ventral prefrontal cortex via the extreme capsule and extending posteriorly along the superior and middle temporal gyri to the posterior temporal lobe.

In humans, probabilistic tracking from the left pMTG seed showed that the ventral white-matter system extends into the right hemisphere via the corpus callosum and into the left dorsal pathways via the connection between the posterior superior temporal sulcus (STS) and the inferior parietal lobe. In chimpanzees, these tractograms were similar with regard to the interhemispheric connections, but connectivity to the dorsal stream was much weaker than in humans. In the right hemisphere, the connectivity patterns mimicked what was found for the left hemisphere in both human and chimpanzees (*SI Appendix*, Fig. S1). The tractograms' visualization (Fig. 1) illustrates overlap between all individuals in order to take into account the intraspecies variability of tractograms' anatomical distribution.

Reconstructing Canonical Tracts. In order to better understand the interspecies differences in ATL and pMTG tractograms, we proceeded to compare their anatomy in relation to seven canonical language tracts. The three portions of the AF—the frontotemporal (in other nomenclatures also known as "direct," "long," or" classical") (reviewed in ref. 12), frontoparietal ("anterior"/"indirect"/"perisylvian"), and parietotemporal ("posterior"/indirect/perisylvian)—were defined anatomically according to Catani et al. (13). This AF "tripartite subdivision" (12) in this work will represent the dorsal stream, while the inferior fronto-occipital fasciculus (IFOF), inferior longitudinal fasciculus (ILF), middle longitudinal fasciculus (MdLF), and uncinate fasciculus (UF) form

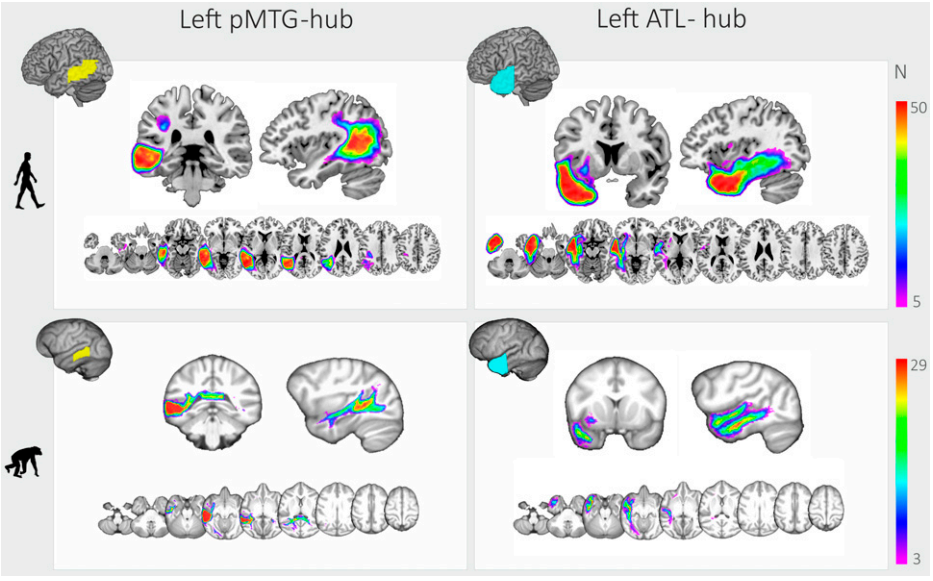

Fig. 1. Overlap of probabilistic tractography results (tractograms) of humans (*Upper*, N = 50) and chimpanzees (*Lower*, n = 29) and left-hemispheric seeds (pMTG: *Left*; ATL: *Right*) from 10% (purple) to 100% (red) of the subjects. Results for the right hemisphere were highly similar to the left and are provided in *SI Appendix*, Fig. S1. Brains are not to scale.

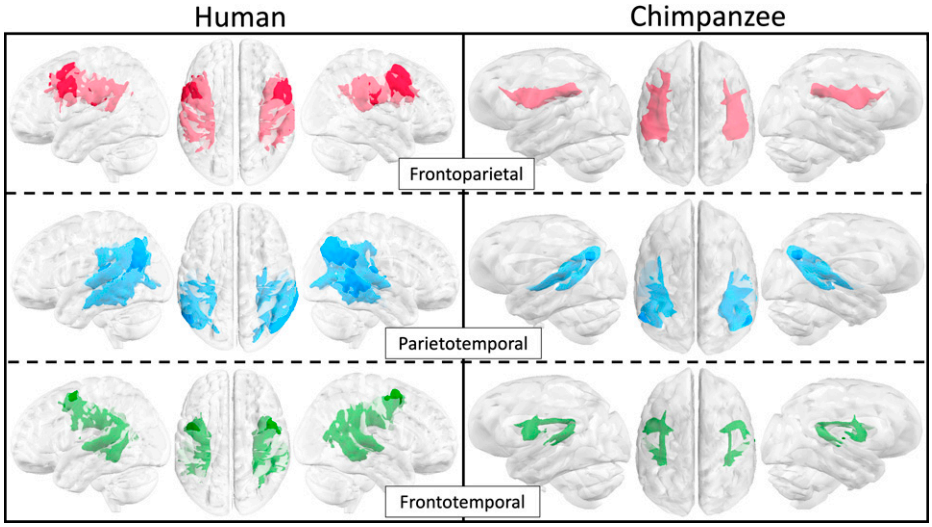

Fig. 2. Mean of the normalized, thresholded tractograms of the three subdivisions of the AF. Brains are not to scale. Images are depicted in neurological convention.

the ventral stream (9, 38). In chimpanzees, ventral canonical tracts were extracted from the white-matter atlas by ref. 21 and calculated according to the recipes proposed by the same authors in the present human sample. The AF subdivisions in humans were reconstructed following previously implemented recipes (13, 39, 40). Subsequently, we adapted the same AF regions of interest (ROIs) in the chimpanzee. This protocol resulted in satisfactory results in both human and chimpanzees. In both species, all three AF portions were present bilaterally, with connections between the frontal and temporal areas and also, branching toward the parietal cortex (Fig. 2 and *SI Appendix*, Fig. S2 have more details).

Quantification of Interspecies Ventral and Dorsal Pathway Similarities. Having examined the connectivity of both pMTG and ATL in both species and characterized the course of all major long-range connections reaching these areas, we next examined the specific contribution of the canonical—dorsal and ventral—tracts to the pMTG and ATL connectivity patterns. For that, we used linear regression analyses on a "tract load" measure defined as the proportion between the volume of the overlap between tractograms created on the basis of pMTG or ATL seeds and each separate canonical tract weighted by the volume of each separate canonical tract (note that all the statistical analyses will be hereafter performed using this dependent variable). At the whole-brain level, quantification of (dis-)similarities indicated a main effect of species for tractography from both pMTG and ATL seeds (P values < 0.001) and an interaction between hemisphere, stream, and species (P values < 0.001) (*SI Appendix*, Tables S1 and S2). Within the left hemisphere, humans and chimpanzees differed significantly in how the seeds connected to the dorsal vs. ventral stream [species by stream interaction; pMTG seed: $F(1,77) = 190.4$, $P < 0.001$; ATL seed: $F(1,77) = 287.5$, $P < 0.001$]. Results concerning the right hemisphere showed similar effects (*SI Appendix*, Tables S1–S3). The differences we found visually (Fig. 1) and statistically (above) were further corroborated by the tract load analysis for each individual tract. For that, we quantified how separate tracts contribute in explaining interspecies differences using separate linear models using the models' R^2 as a measure of effect size.

For both hemispheres, the interspecies differences for the pMTG seed we observed were best explained by tracts forming the dorsal stream (AF) and in particular, the parietotemporal branch (left $R^2 = 0.71$, $P < 0.001$; right $R^2 = 0.7$, $P < 0.001$). Species also explained the variance for the pMTG connections toward the ventral tracts. However, within this stream, humans showed more overlap with pMTG tractograms only for the left MdLF (left $R^2 = 0.45$, $P < 0.001$). Conversely, ILF, IFOF, and UF overlapped more strongly with the pMTG in the chimpanzees in both left ($R^2 = 0.5$, $P < 0.001$; $R^2 = 0.36$, $P < 0.001$; and $R^2 = 0.24$, $P < 0.001$, respectively) and right ($R^2 = 0.43$, $P < 0.001$; $R^2 = 0.53$, $P < 0.001$; and $R^2 = 0.37$, $P < 0.001$, respectively) hemispheres. For the left ATL, there was no interspecies difference in connectivity with any of the AF portions, whereas the ventral tracts differed between species, with the exception of the IFOF. For the left ATL seed, species explained the variance in tract load for the following canonical ventral tracts: ILF ($R^2 = 0.9$, $P < 0.001$), UF ($R^2 = 0.49$, $P < 0.001$), and MdLF ($R^2 = 0.42$, $P < 0.001$). Results in the right hemisphere were similar. The contribution of specific tracts to the interspecies difference is specified in Fig. 3.

Discussion

We reassessed the connectional basis of language in the light of developments in both our understanding of language and the emergence of increasingly high-quality comparative neuroimaging data and methods. Using a large high-quality in vivo chimpanzee dataset, we show that dorsal connectivity of the pMTG to both frontal and parietal cortices is much more extensive in the human brain. By directly comparing the organization of the pMTG- and ATL-based tractograms between the species (and accounting for both intra- and interspecies variability), we were able to identify structural changes that are unique to humans and may have laid the foundation for full-fledged language in the human lineage.

Additionally, we detected that AF in chimpanzees obeys the same threefold division as in humans, with one large connection between frontal and temporal lobes and two shorter ones: frontoparietal and parietotemporal.

Between-Species Differences in pMTG Connectivity. Our results on the pMTG-related white-matter connections in humans are in line with previous anatomical findings by Turken and Dronkers (36), with tractograms encompassing extensive portions

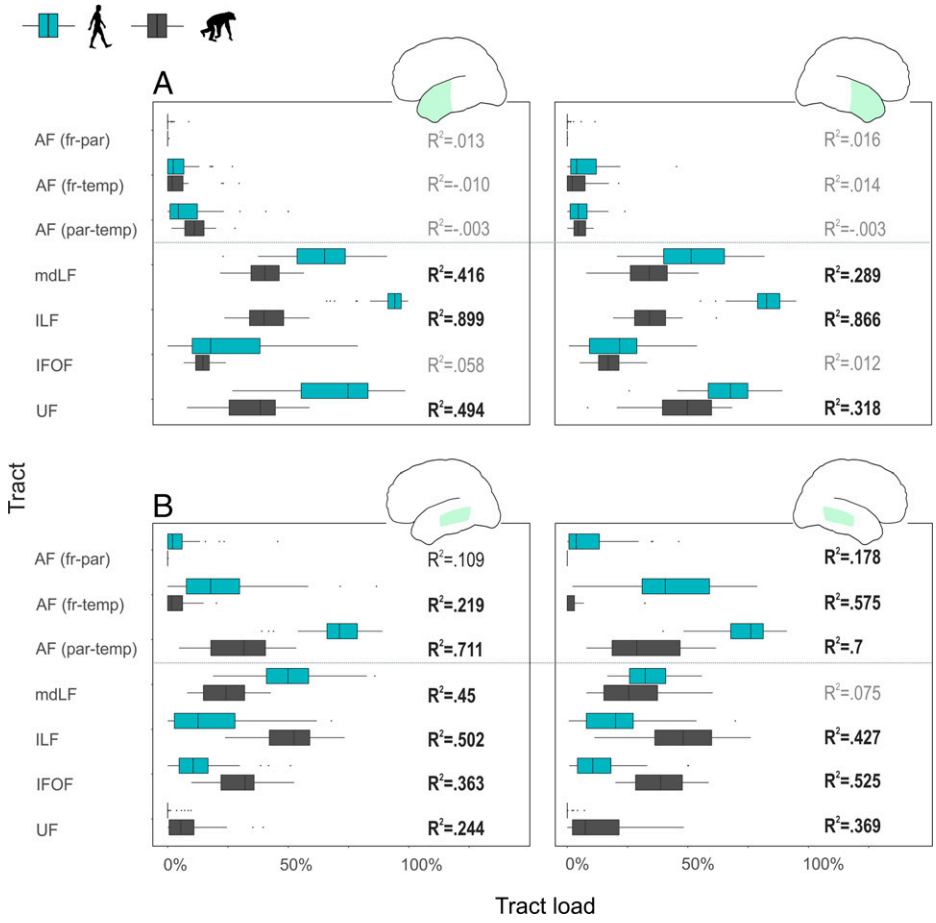

Fig. 3. Box plots of the tract load and statistical differences between species for tract loads of tractograms originating from ATL and pMTG (tract loads were quantified as a proportion between the overlap of the seed-related tractograms and each specific canonical tract weighted by the volume of each canonical tract). Turquoise bars, human; gray bars, chimpanzee. (*A*) ATL tract loads; (*B*) pMTG tract loads. (*A*, *Left* and *B*, *Left*) Left hemisphere. (*A*, *Right* and *B*, *Right*) Right hemisphere. Adjusted R^2 values are shown on the right side of each pair of bars (in gray when the *P* value is >0.05, in black when the *P* value is =0.02, and in bold for when the *P* value is <0.001). All *P* values are corrected for multiple comparisons using Holm's method. fr, frontal; par, parietal; temp, temporal.

of temporal and parietal lobes. Importantly, our analysis of chimpanzees confirmed the uniqueness of the human expansion of the dorsal language tracts. In humans, tractograms originating from the pMTG overlapped with all temporo-parietofrontal connections of the AF, whereas the same tractograms in chimpanzees were confined mainly to the temporal lobe. Further, pMTG connectivity differed in the ventral pathway; with the exception of the MdLF, the overlap between the pMTG tractogram and the ventral language stream was stronger in chimpanzees than in humans.

A plethora of studies indicates that pMTG has a unique role in human language. It has been repeatedly postulated to act as a lexical hub (2, 10, 30, 38). It is also well established that damage to pMTG can induce paragrammatism and can impair object naming and/or impede (syntactic) comprehension [e.g., due to the presence of brain tumors (41) or after stroke (23, 42, 43)]. Functional studies have demonstrated that the pMTG mediates the functional integration of novel words into the mental lexicon (e.g., refs. 44–46), and previous evolutionary neuroscience studies have shown that this area has a human-unique pattern of white-matter connectivity (1, 22). Importantly, the evolutionary development of pMTG as a white-matter hub accommodating new connections between frontal and temporal regions aligns well with observations from human development. Indeed, early in life—before language is acquired—the structural connection between frontal and temporal cortices is vastly underdeveloped, joining premotor regions solely to the most superior portions of the temporal cortex (47). In these newborns, there is also no functional connectivity between frontal and temporal regions. For older children, the AF remains immature at the age of seven (48), whereas AF volume and fractional anisotropy both increase with age in adolescence (49). A robust connection between inferior frontal and deep temporal areas (including middle and inferior gyri) through the AF is found only in adulthood (47). Interestingly, other evidence supports the crucial role of the AF in language/cognitive abilities, such as phonological processing (50–52), language learning (39), naming and speech rate and efficiency (53, 54), or even singing and musical training (55). In our study, the observed broad expansion of pMTG connectivity in humans is mainly explained by two branches of the AF—the frontotemporal branch and especially, the parietotemporal branch. Importantly, these effects are present even when taking intraspecies variability into account. These findings suggest that, as the AF expanded in human evolution, the modifications were concentrated in the frontoparietal and parietotemporal branches and further, that the bundle connecting pMTG to parietal areas underwent particularly strong selection.

The parietotemporal connection of the AF in humans is of special interest because of its putative role in language learning. Evidence suggests that the connection between the pMTG and inferior parietal cortex permits phonological information to be held in working memory (56, 57) as part of the larger phonological loop system (58). Recent work suggests that this parietotemporal portion may control information about the order of phonological

information, while the frontoparietal component is involved in transferring this order information to portions of the left inferior frontal gyrus (59). Further, there is evidence for human-unique differences in structure, as asymmetry of the thickness of the STS has been documented in humans but not in chimpanzees (60). Although we observed trends that frontotemporal AF tractograms explained more variance in the right hemisphere compared with the left, interspecies differences were statistically significant in both hemispheres. Therefore, with the present results we cannot claim clear species differences in laterality.

Human ATL Connectivity Specializations. Like the pMTG, the ATL has been postulated to have a crucial role in language as a semantic hub. Indeed, "the hub-and-spoke" model by ref. 35 proposes that the left ATL is involved in binding together perceptually-based semantic representations into coherent concepts. For this reason, we explored whether ATL-related white-matter organization could also differ between humans and chimpanzees. In an opposite pattern to pMTG connectivity and as to be expected, the left ATL scarcely connected with AF in either species, but ventral pathway connectivity was significantly different for nearly all relevant tracts. When comparing humans with chimpanzees, ILF, MdLF, and UF were the best predictors of interspecies differences with regard to the left ATL connectivity. The ILF is a large association tract that has expanded laterally in the human and great ape lineage (28). The degeneration of ILF can produce semantic and lexical retrieval difficulties (reviewed in ref. 61). The UF connects the ATL to orbitofrontal cortex and plays a role in semantic and syntactic functions (62, 63). Although direct stimulation of the UF does not appear to cause language errors (64), lesions to the tract are linked to lexical deficits (65, 66). The pattern of connections was similar in the right hemispheres (Fig. 3).

Ventral Pathway Modifications. MdLF has increasingly been implicated in language processing (9, 67, 68), but its connectivity to human language hubs has never been compared with its connectivity to analogous regions in other species. Here, our direct comparison between human and chimpanzee showed that the MdLF is the only tract showing human-unique expansions in both ATL and pMTG hubs.

Tractograms from pMTG appeared to be more strongly integrated with IFOF in the chimpanzees (Fig. 1), while IFOF connectivity to ATL was low in both species. In chimpanzees, three of the four ventral pathway tracts (ILF, IFOF, and UF) showed a greater proportion of connectivity to pMTG than in humans, while the reverse pattern was observed in the ATL. Given these anatomical findings and previous evidence that the ATL/IFOF system plays an important role in conceptual processing [e.g., humans (69) or vervet monkeys (70)], our results add light to the view that concepts rely on a white-matter structure that is shared between humans and other primates. Reweighting of ventral pathways with respect to the two species may also reflect recruitment of areas originally used for visual processing in the pMTG in humans for language processing. The larger contribution of IFOF and ILF to chimpanzee pMTG connectivity may be due to its anatomical location adjacent to visual association areas (*Additional Considerations*). Overall, these data provide more details on the relationship between ventral pathways and the temporal association cortex in humans and chimpanzees, which has only recently been characterized using comparative neuroimaging (21, 71).

Additional Considerations. Our initial claims stemmed from a theory-driven interest in left-hemispheric temporal lobe connectivity; however, to gain insight into whether these patterns were consistent across hemispheres, we ran the same analyses for the right hemisphere. We found similar results, suggesting that modifications to white-matter organization in humans occurred bilaterally. Further, frontotemporal tracts loaded slightly higher on the right hemisphere human pMTG than the left hemisphere; however, our study was not designed to test between-hemisphere differences. In recent decades, evidence for right hemisphere specializations has been accumulating, especially with regard to the role of right parietofrontal circuits in tool action planning (72) and toolmaking (73, 74), behaviors that are relevant to human evolution. Our findings are consistent with the possibility that language and tool use may rely on similar modifications of dorsal pathways in the human brain occurring in the left and right hemispheres, respectively.

In addition to tool-related cognitive processing, there is evidence that pMTG and ATL are important for other behaviors beyond language in humans. The pMTG has been implicated in object motion processing, possibly due to its proximity to visual motion area MT+ (75, 76). The ATL is involved in semantic and affective cognition, including picture recognition, gustatory and olfactory memory, emotional memory, and storage of socially-relevant entities (reviewed in ref. 77). Thus, the putative evolutionary processes causing the reweighting of dorsal and ventral tract connectivity to pMTG and the increase of ventral tract connections to ATL in humans may have been due to selection for modifications in tool-related cognition, affective cognition, and forms of semantic processing that are not limited to language.

Determining the homologous cortical territories in chimpanzees for human pMTG and ATL is challenging because the methods available for delineating these regions in humans (functional Magentic Resonance Imaging (fMRI) and in some clinical cases, direct stimulation) are not feasible in apes. We, therefore, rely on previous structural data from chimpanzees, including cortical parcellations (e.g., ref. 78), sulcal maps (79), tractography of extrastriate and temporal areas (21, 27), and myelin maps (77). It is worth mentioning that our ROIs for humans and chimpanzees were similar but not identical in proportion to the total intracranial volume, with chimpanzee ROIs making up a smaller proportion (*Methods*). However, this should not bias our results for two reasons. First, the ROIs are confined to association cortex, which has expanded disproportionately in humans compared with great apes and other primates (80, 81). Second, our core analysis relies on an analysis of proportion of tract loads in relation to ROIs rather than absolute volumes.

Comparative anatomical studies endeavor to identify putative evolutionary modifications to the brain; however, they cannot determine the mechanisms that are responsible for the differences in neuroanatomy. As such, we cannot disambiguate whether these differences in connectivity are environmentally or genetically driven or (most likely) are a combination. In order to shed light on these interlinked factors, future studies are needed that compare individuals between species across the life span. In the case of chimpanzees, neuroanatomical comparisons of individuals from different environments (i.e., captive vs. wild populations) may also shed light on how natural selection shaped human brains by permitting the characterization of the flexibility of development and the amount of individual variation in connectivity there may be within this species.

Conclusions

The results of our study indicate that two hubs critical for language, pMTG and ATL, have undergone changes in their connectivity since our evolutionary divergence from chimpanzees.

We found that, compared with chimpanzees, human pMTG has expanded AF connectivity, with the largest increase in the parietotemporal branch, and decreased ventral pathway connectivity, particularly with ILF and IFOF. Human ATL has more robust connections with ventral pathways, with the exception of the IFOF. Finally, MdLF is the only tract showing interspecies differences for both ATL and pMTG hubs. Together, these data suggest that the evolutionary modifications to human language streams not only encompass the AF but rather, include an increase of dorsal stream connectivity to pMTG and ventral stream connectivity to ATL with a concomitant reduction in ventral stream connectivity to the pMTG.

Methods

Sample. High-resolution DWI data for 50 healthy human subjects (mean age = 43.7 ± 21.6 y) were acquired using a Siemens Prisma Fit 3T scanner and a 32-channel head coil at the Donders Center for Cognitive Neuroimaging, Nijmegen. Diffusion-weighted images were acquired with a simultaneous multislice diffusion-weighted echo planar imaging (EPI) sequence. Acquisition parameters were the following: multiband factor = 3; TR (repetition time) = 2,282 ms; TE (echo time) = 71.2 ms; in-plane acceleration factor = 2; voxel size = 2 × 2 × 2 mm^3; nine unweighted scans; 100 diffusion-encoding gradient directions in multiple shells; b values = 1,250 and 2,500 s/mm^2; and Taq (total acquisition time) = 8 min, 29 s. A high-resolution T1 anatomical scan was obtained for spatial processing of the DWI data using the MP2RAGE sequence (82) with the following parameters: 176 slices; voxel size = 1 × 1 × 1 mm^3; TR = 6 s; TE = 2.34 ms; and Taq = 7 min, 32 s. MP2RAGE data were processed using the Oxford Center for Functional Magnetic Resonance Imaging of the Brain (FMRIB) software library (FSL 5.0.10; https://www.fmrib.ox.ac.uk/fsl) and skull stripped with Brain Extraction Tool (BET). DWI images were preprocessed to realign and correct for eddy current (using Statistical Parametric Mapping software - SPM12) and for artifacts from head and/or cardiac motion using robust tensor modeling [Donders Institute Diffusion Imaging toolbox (83)]. After preprocessing, diffusion parameters were estimated at each voxel using BedpostX. Tensor reconstruction using weighted least squares fit was performed via Diffusion Tensor Imaging fitting (DTIFit) within FMRIB's Diffusion Toolbox (FDT) to create Diffusion Tensor Imaging (DTI scalar images, including the fractional anisotropy (FA), mean diffusivity (MD), and three eigenvalues [FSL 5.0.10 (84)]. This study was approved by the local ethics committee (Commissie Mensgebonden Onderzoek (CMO, i.e., the Committee for Ethics of Research on Humans) Arnhem-Nijmegen, "Imaging Human Cognition," CMO 2014/288). Subjects provided informed consent.

Diffusion-weighted data from 29 chimpanzees (*Pan troglodytes*; 28 ± 17 y) were obtained from a data archive of scans obtained prior to the 2015 implementation of US Fish and Wildlife Service and NIH regulations governing research with chimpanzees. These scans were made available through the United States–based National Chimpanzee Brain Resource. All scans reported here were completed in 2012 and have been used in previous studies (e.g., refs. 21 and 27). Chimpanzees were housed at the Yerkes National Primate Research Center (YNPRC) in Atlanta, GA; procedures were carried out in accordance with protocols approved by the YNPRC and the Emory University Institutional Animal Care and Use Committee (approval no. YER-2001206). Following standard YNPRC veterinary procedures, chimpanzee subjects were immobilized with ketamine injections (2 to 6 mg/kg intramuscular) and then, anesthetized with an intravenous propofol drip (10 mg/kg per hour) prior to scanning. Subjects remained sedated for the duration of the scans and the time necessary for transport between their home cage and the scanner location. After scanning, primates were housed in a single cage for 6 to 12 h to recover from the effects of anesthesia before being returned to their home cage and cage mates. The well-being (activity and food intake) of chimpanzees was monitored twice daily after the scan by veterinary staff for possible postanesthesia distress.

Anatomical and diffusion MRI scans were acquired in a Siemens 3T Trio scanner (Siemens Medical System). A standard circularly polarized birdcage coil was used to accommodate the large chimpanzee jaw, which does not fit in the standard phase-array coil used in humans. DWI data were collected with a single-shot, spin-echo EPI sequence; to minimize eddy-current effects, a dual spin-echo technique combined with bipolar gradients was used. Parameters were as follows; 41 slices were scanned at a voxel size of 1.8 × 1.8 × 1.8 mm, TR/TE was 5,900/86 ms, and matrix size was 72 × 128. Two DWI images were acquired for each of 60 diffusion directions, each with one of the possible left–right phase-encoding directions and eight averages, allowing for correction of susceptibility-related distortion (85). For each average of DWI images, six images without diffusion weighting (b = 0 s/mm^2) were also acquired with matching imaging parameters. High-resolution T1-weighted MRI images were acquired with a three-dimensional magnetization-prepared rapid gradient-echo sequence for all subjects. T2 images were previously acquired (86) using parameters similar to a contemporaneous study on humans (87).

Data preprocessing was achieved using the FSL software library of the FMRIB (https://www.fmrib.ox.ac.uk/fsl) (88). T1-weighted images were skull stripped with BET with some manual correction (89). To correct for eddy current and susceptibility distortion, FSL's eddy_correct (90) and topup (85) implemented in MATLAB (MATLAB7; MathWorks) were used. FMRIB's Diffusion Toolbox (FDT) was used to fit diffusion tensors, estimate mean diffusivity and fractional anisotropy, and run bedpostX to fit a voxel-wise model of diffusion tensors using a crossing fiber model with three fiber directions (91). A modified version of the Human Connectome Project minimal preprocessing pipeline (92) was used to create registrations to a population-specific chimpanzee template.

Template generation for chimpanzees has been previously described (93, 94); briefly, the PreFreeSurfer pipeline was used to align the T1w and T2w volumes of 29 individual chimpanzees to native anterior commissure–posterior commissure space. FSL was used to perform brain extraction, cross-modal registration, bias field correction, and nonlinear volume registration to atlas space.

ROI Definition. For human participants, two binary masks were defined within the Montreal Neurological Institute (MNI) space using the SPM Marsbar extraction tool and the Automated Anatomical Labeling (AAL) atlas: the pMTG and the ATL (for both the left and right hemispheres separately). The pMTG mask was defined by restricting the middle temporal gyrus to its portion located posteriorly to the central sulcus [$y = -18$ according to the methodology proposed by Turken and Dronkers (36)] (*SI Appendix*, Fig. S2). The ATL mask was obtained by joining five parts: the middle and superior temporal poles and the anterior portions of the inferior, middle, and superior temporal gyri (terminating at $y = -17$). Subsequently, the masks were transferred to each individual's diffusion space, where the voxels in the mask that had a 90% probability of being present in the original mask were included. This conservative threshold of 90% was chosen to ensure that there was no overlap between the ATL and pMTG masks in the same participant. Afterward, the masks were binarized. In chimpanzees, a similar protocol was followed, with masks manually drawn in the chimpanzee template corresponding to human areas using homologous sulcal and gyral landmarks in chimpanzees using recent sulcal/gyral maps for this species (79). Importantly for the delineation of the ATL ROI, the central sulcus in chimpanzees is substantially more angled than in humans. For this reason, the central point of the central fissure was chosen as a reference; slices were counted in the coronal direction, and the midpoint was set along the sulcus as a cutting point for defining the posterior and anterior temporal lobes ($y = -15$).

For the delineation of the pMTG ROI in the chimpanzee, we considered three alternative options of its posterior limit: 1) the posterior edge of the Sylvian fissure; 2) the descending ramus of the STS, and 3) the limit defined according to a chimpanzee brain atlas (78) (*SI Appendix*, Fig. S3); we chose the second option as the most suitable to reproduce human anatomy. Here, the posterior limit of the chimpanzee pMTG ROI was delineated at the descending ramus of the STS, which is an approximation of the boundary between the unimodal extrastriate cortex and the multimodal association cortex based on previous studies (27, 77). Subsequently, we compared the tractograms obtained with the three alternative ROIs to test if the modifications provoke significant impact on the final results. From visual inspection, the tractograms were only minimally different (and in both hemispheres) (*SI Appendix*, Fig. S4), which ensured that choosing ROIs according to fixed anatomical landmarks was appropriate. Statistical analyses showed that neither of the ROIs including multimodal association cortex only (options 1 and 2) showed human advantage in connectivity between pMTG and three major ventral tracts (UF, ILF, and IFOF). Moreover, the ROI extending until the limit with the unimodal extrastriate cortex (option 2, reported here) revealed that the three above-mentioned tracts showed statistically higher levels of

overlap with pMTG in the chimpanzees. All remaining steps in ROIs' transformation toward their individual diffusion space were kept the same as for humans (*SI Appendix*, Fig. S2).

Once the masks were obtained, we extracted their volume for humans and chimpanzees and weighted this measurement by the volume of the template used for their delineation (i.e., gray- and white-matter MNI template and the chimpanzee template, respectively). In humans, the masks took up the following proportions of brain template volume–pMTG: 0.018 (left) and 0.016 (right) and ATL: 0.025 (left) and 0.031 (right). In the chimpanzee, the masks occupied the following proportions–pMTG: 0.008 (left) and 0.009 (right) and ATL: 0.018 (both left and right).

Mean and Overlap of the Tractograms. For both humans and chimpanzees, white-matter connections stemming from the ROIs were calculated using a probabilistic approach (FSL probtrackx) for both ROIs and both hemispheres separately. Tracking was initiated from all voxels within the seed masks to generate 10,000 streamline samples, with a curvature threshold of 0.2 and a 0.5-mm step length. The resulting connectivity maps were thresholded at 99% of the robust range and binarized. From these connectivity maps, two output images were calculated–the mean connectivity map of all the participants and the sum (overlap) of the connectivity maps of all participants, showing the per-participant overlap in tractography distributions. To better account for the interindividual variability, we present the visualization of the overlap maps in Fig. 1.

Definition of the Canonical Ventral and Dorsal Pathways for Language. Once the white-matter tractograms related to the two seeds (pMTG and ATL) were defined for each individual (human and chimpanzee), we proceeded to define the canonical white-matter tracts with a well-established role in language: the three portions of the AF (frontoparietal, frontotemporal, and parietotemporal) (13), IFOF, ILF, UF, and MdLF. In humans, the tracts were defined in a semiautomated manner, inputting the ROIs defined within the MNI space and using the autoptx [now renamed XTRACT and allowing cross-species tractography (20)] algorithms as part of the probabilistic approach (FSL probtrackx). In order to virtually dissect the three branches of AF, three different two-ROI combinations were applied as seed and target masks. The ROIs were defined in the frontal, temporal, and parietal areas, and their combinations formed frontotemporal (also called long), frontoparietal (also called anterior), and parietotemporal (also called posterior) branches of the AF. The ROI for the frontal area was placed in the coronal plane between the central sulcus and the inferior frontal gyrus. The ROI for the temporal area was placed in the axial plane at the level of white matter descending to the posterior temporal lobe through the posterior portion of the temporal stem. The parietal ROI was defined at the sagittal plane encompassing the angular and supramarginal gyri of the inferior parietal lobe (more details are in ref. 39). This process was carried out for both the left and right hemispheres. Additionally, an exclusion mask was added to the AF analyses, encompassing the midline (sagittal slice), thalami, basal ganglia, and portions of the third and lateral ventricles. Subsequently, the ROIs were adapted to the population-specific chimpanzee template informed by previous work on chimpanzee arcuate neuroanatomy (1, 21).

To define the ventral stream, we implemented tractography protocols used in humans and recently adapted specifically for chimpanzees for reconstructing IFOF, ILF, MdLF, and UF, which are described in detail in Bryant et al. (21). Briefly, the MdLF was reconstructed using seed and target masks in superior temporal gyrus (STG) white matter, with exclusion masks placed in the middle temporal gyrus (MTG), the inferior temporal gyrus (ITG), and the prefrontal cortex. For the ILF, masks were inverted from the MdLF protocol; seed and target masks were placed in the white matter within the MTG and ITG, and exclusion masks were placed in the STG as well as the hippocampal formation, amygdala, and the cerebellar peduncle. In humans, the ILF target mask was moved posteriorly to the level of the angular gyrus, with an additional axial slice in the inferior parietal lobule. IFOF protocols involved a large coronal slice in the occipital lobe for the seed, a coronal slice in the prefrontal cortex as the target, and a coronal slice with two lacunae at the extreme/external capsule as the exclusion mask. The UF protocol used the same exclusion mask as the IFOF along with an ATL seed and a target in the extreme/external capsule. A second exclusion mask was placed posterior to the basal ganglia. The advantage of defining the ROIs within the MNI space was twofold. First, it assured that the seeds were defined in the same way for every individual; second, it allowed us to reliably replicate the same steps of the analyses between the two species. After the visual inspection of the autoptx results (already corrected for the size of the seeds and densityNorm), the tracts were thresholded at 99% of the robust range and binarized (with default threshold). In chimpanzees, all the steps of the analyses were kept the same as for humans. The three portions of the AF will be further considered as representative of the dorsal stream, whereas the IFOF, ILF, UF, and MdLF will represent the ventral stream.

Calculation of the Contribution of the Canonical Tracts to the Language Hubs. To define the extent of overlap between the pMTG and ATL tractograms and the canonical tracts, normalized, thresholded, and binarized pMTG and ATL tractograms (separately) were multiplied by each of the normalized, thresholded, and binarized canonical tracts. This step resulted in 14 values per participant (or chimpanzee) per hemisphere (pMTG × frontoparietal AF, pMTG × parietotemporal AF, pMTG × frontotemporal AF, pMTG × IFOF, pMTG × ILF, pMTG × UF, pMTG × MdLF, ATL × frontoparietal AF, ATL × parietotemporal AF, ATL × frontotemporal AF, ATL × IFOF, ATL × ILF, ATL × UF, ATL × MdLF). Seven additional values were extracted to represent the absolute volume of the canonical tracts to correct the measure for canonical tract size [i.e., the volume of (tractogram binary mask × canonical binary mask)/the volume of the canonical tract binary mask]. These steps resulted in a measure of the contribution of the canonical tracts to the pMTG and ATL seed-related white-matter tractograms. Throughout the manuscript, we refer to these proportions of overlap as the tract loads.

Statistical Analyses. For inferential statistics, the tract loads were specified as dependent variables. Stream (dorsal vs. ventral, within subject), hemisphere (left vs. right, within subject), and species (human vs. chimpanzee, between subjects) were defined as independent variables. In addition, two streams were composed of specific tracts: the dorsal stream (three portions of the AF: frontoparietal AF, frontotemporal AF, parietotemporal AF) and the ventral stream (IFOF, ILF, UF, MdLF). First, a repeated-measures ANOVA was performed for each of the seeds separately to test if the tract loads differed as a function of hemisphere, stream, and species (including their interactions). Following up on significant interactions, repeated-measures ANOVAs were performed within each hemisphere and seed to examine if the species differed with respect to stream (dorsal vs. ventral). Finally, the contribution of each tract load to explaining the interspecies difference was quantified using 28 linear regressions (seven tracts, two hemispheres, two seeds). Adjusted R^2 values of the models were used as a measure of effect size of each tract's ability to explain the interspecies differences (all 28 P values were corrected for family-wise error rate due to multiple comparisons using the Holm method). The analyses were performed using R studio (version 3.5.3; R Core Team 2019) and tidyverse (95), broom (96), and purrr (97) packages.

Methodological Considerations. Diffusion MRI tractography is a relatively new tool for comparative neuroscience. Although it has been criticized when compared directly with more traditional neuroscientific methods, it has shown to be replicable, and further, it has clear advantages for comparative analyses. When compared with tract tracing, diffusion tractography in ex vivo macaques found comparable results (98–101). The present investigation uses high–angular resolution data, which have been shown to perform well on difficult to reconstruct tracts like the acoustic radiation (98); further, multifiber algorithms increase sensitivity (91).

Size and scan resolution differences are important to take into account in comparative anatomical studies; this dataset is the highest-quality in vivo chimpanzee dataset available and has been previously shown to perform favorably in comparison with human and macaque datasets (21). Additionally, tractograms are normalized after averaging to minimize the impact of differences in brain size and resolution between the two species.

Another challenge of comparative neuroanatomy is to determine whether tracts have increased or decreased in size and whether this is relative to cortex volume, white-matter volume, other tracts, or the size of functional areas. Ultimately, this is not possible to disentangle, as it is not possible to reconstruct the anatomy of the common ancestor of humans and chimpanzees. However, it is possible to directly compare extant species, making the least assumptions about structural homologies and relying on the closest direct anatomical observation. Since chimpanzees not only have a brain roughly one-third the size of humans but also, have different proportions of gray and white matter (as those scale differently from one another as brain size increases across mammals), directly comparing volumes tract by tract between humans and other primates would be

unsuitable. Thus, to make the least number of assumptions is to rely on the relative sizes of tracts within species to anchor our analysis, as in previous comparative Diffusion Tensor Imaging (DTI) work (102).

The best way to mitigate possible false positives is to use strong anatomical priors (103). Here, we adapted previously validated human tractography protocols to the chimpanzee using a chimpanzee white-matter atlas (21) that, in turn, was based on strong anatomical knowledge from other species, including the macaque. The tractography procedure is the same for both species, which have similar gyrification indices and in principle, should have similar vulnerability to gyral bias (104). This results in a like with like comparison that is the best for comparative neuroanatomical studies and preferable to comparing different methodologies (e.g., comparing tracer and tractography data) (105).

Data Availability. Thresholded and binarized white matter tractograms, ROIs (AF, pMTG and ATL), a dataset containing tract loads and code to reproduce the results have been deposited in Donders Repository (https://doi.org/10.34973/warf-df84) (106).

ACKNOWLEDGMENTS. We thank Roy P. C. Kessels and Ardi Roelofs for the funding that enabled the acquisition of the human DWI data as well as Federico Varriano and Alberto Prats-Galino for sharing their expertise on brain anatomy.

This study was supported by Netherlands Organization for Scientific Research (NWO) Grants 452-13-015 (to R.B.M.), 451-17-003 (to V.P.), and 024-001-006 (to the Language in Interaction Consortium). The acquisition of the human DWI data was funded by NWO Gravitation Grant 024.001.006 of the Language in Interaction Consortium (to Roy P. C. Kessels and Ardi Roelofs). K.L.B. is supported by European Commission Marie Sklodowska-Curie Postdoctoral Research Fellowship MSCA-IF 750026 (to K.L.B.) and Biotechnology and Biological Sciences Research Council (BBSRC) UK Grant BB/N019814/1 (to R.B.M.). R.B.M. is also supported by BBSRC UK Grant BB/N019814/1. The Wellcome Centre for Integrative Neuroimaging is supported by core funding from Wellcome Trust Grant 203129/Z/16/Z. This research was funded in whole or in part by the Wellcome Trust.

Author affiliations: [a]Donders Institute for Brain, Cognition and Behaviour, Radboud University, 6500 GL Nijmegen, the Netherlands; [b]Donders Centre for Medical Neuroscience, Department of Medical Psychology, Radboud University Medical Center, 6500 HB Nijmegen, the Netherlands; [c]Wellcome Centre for Integrative Neuroimaging, Centre for Functional MRI of the Brain, Nuffield Department of Clinical Neurosciences, John Radcliffe Hospital, University of Oxford, Oxford OX3 9DU, United Kingdom; [d]Department of Psychiatry, Radboud University Medical Center, 6525 GA Nijmegen, the Netherlands; [e]Department of Cognitive Neuroscience, Radboud University Medical Centre, 6500 HB Nijmegen, the Netherlands; and [f]Institute for Science in Society, Radboud University, 6525 AJ Nijmegen, the Netherlands

1. J. K. Rilling *et al.*, The evolution of the arcuate fasciculus revealed with comparative DTI. *Nat. Neurosci.* **11**, 426–428 (2008).
2. A. Roelofs, A dorsal-pathway account of aphasic language production: The WEAVER++/ARC model. *Cortex* **59**, 33–48 (2014).
3. M. R. Schomers, M. Garagnani, F. Pulvermüller, Neurocomputational consequences of evolutionary connectivity changes in Perisylvian language cortex. *J. Neurosci.* **37**, 3045–3055 (2017).
4. J. K. Rilling, M. F. Glasser, S. Jbabdi, J. Andersson, T. M. Preuss, Continuity, divergence, and the evolution of brain language pathways. *Front. Evol. Neurosci.* **3**, 11 (2012).
5. A. D. Friederici, Pathways to language: Fiber tracts in the human brain. *Trends Cogn. Sci.* **13**, 175–181 (2009).
6. F. Corbett, E. Jefferies, S. Ehsan, M. A. Lambon Ralph, Different impairments of semantic cognition in semantic dementia and semantic aphasia: Evidence from the non-verbal domain. *Brain* **132**, 2593–2608 (2009).
7. A. R. Bradshaw, P. A. Thompson, A. C. Wilson, D. V. M. Bishop, Z. V. J. Woodhead, Measuring language lateralisation with different language tasks: A systematic review. *PeerJ* **5**, e3929 (2017).
8. Z. V. J. Woodhead, A. R. Bradshaw, A. C. Wilson, P. A. Thompson, D. V. M. Bishop, Testing the unitary theory of language lateralization using functional transcranial Doppler sonography in adults. *R. Soc. Open Sci.* **6**, 181801 (2019).
9. D. Saur *et al.*, Ventral and dorsal pathways for language. *Proc. Natl. Acad. Sci. U.S.A.* **105**, 18035–18040 (2008).
10. G. Hickok, D. Poeppel, Dorsal and ventral streams: A framework for understanding aspects of the functional anatomy of language. *Cognition* **92**, 67–99 (2004).
11. N. Geschwind, The organization of language and the brain. *Science* **170**, 940–944 (1970).
12. L. Vavassori, S. Sarubbo, L. Petit, Hodology of the superior longitudinal system of the human brain: A historical perspective, the current controversies, and a proposal. *Brain Struct. Funct.* **226**, 1363–1384 (2021).
13. M. Catani, D. K. Jones, D. H. ffytche, Perisylvian language networks of the human brain. *Ann. Neurol.* **57**, 8–16 (2005).
14. P. Hagoort, The neurobiology of language beyond single-word processing. *Science* **366**, 55–58 (2019).
15. P. Friedrich *et al.*, Imaging evolution of the primate brain: The next frontier? *Neuroimage* **228**, 117685 (2021).
16. PRIMatE Data Exchange (PRIME-DE) Global Collaboration Workshop and Consortium, Accelerating the evolution of nonhuman primate neuroimaging. *Neuron* **105**, 600–603 (2020).
17. R. B. Mars *et al.*, Whole brain comparative anatomy using connectivity blueprints. *eLife* **7**, e35237 (2018).
18. M. P. van den Heuvel, E. T. Bullmore, O. Sporns, Comparative connectomics. *Trends Cogn. Sci.* **20**, 345–361 (2016).
19. R. B. Mars *et al.*, Primate comparative neuroscience using magnetic resonance imaging: Promises and challenges. *Front. Neurosci.* **8**, 298 (2014).
20. S. Warrington *et al.*, XTRACT: Standardised protocols for automated tractography in the human and macaque brain. *Neuroimage* **217**, 116923 (2020).
21. K. L. Bryant, L. Li, N. Eichert, R. B. Mars, A comprehensive atlas of white matter tracts in the chimpanzee. *PLoS Biol.* **18**, e3000971 (2020).
22. N. Eichert *et al.*, Cross-species cortical alignment identifies different types of anatomical reorganization in the primate temporal lobe. *eLife* **9**, 9 (2020).
23. F. Balezeau *et al.*, Primate auditory prototype in the evolution of the arcuate fasciculus. *Nat. Neurosci.* **23**, 611–614 (2020).
24. C. Girard-Buttoz *et al.*, Chimpanzees use numerous flexible vocal sequences with more than two vocal units: A step towards language? bioRxiv [Preprint] (2021). https://doi.org/10.1101/2021.02.03.429517 (Accessed 29 March 2021).
25. S. S. Keller, N. Roberts, W. Hopkins, A comparative magnetic resonance imaging study of the anatomy, variability, and asymmetry of Broca's area in the human and chimpanzee brain. *J. Neurosci.* **29**, 14607–14616 (2009).
26. N. M. Schenker *et al.*, Broca's area homologue in chimpanzees (*Pan troglodytes*): Probabilistic mapping, asymmetry, and comparison to humans. *Cereb. Cortex* **20**, 730–742 (2010).
27. K. L. Bryant *et al.*, Organization of extrastriate and temporal cortex in chimpanzees compared to humans and macaques. *Cortex* **118**, 223–243 (2019).
28. L. Roumazeilles *et al.*, Longitudinal connections and the organization of the temporal cortex in macaques, great apes, and humans. *PLoS Biol.* **18**, e3000810 (2020).
29. A. Rodríguez-Fornells, T. Cunillera, A. Mestres-Missé, R. de Diego-Balaguer, Neurophysiological mechanisms involved in language learning in adults. *Philos. Trans. R. Soc. Lond. B Biol. Sci.* **364**, 3711–3735 (2009).
30. D. W. Gow Jr., The cortical organization of lexical knowledge: A dual lexicon model of spoken language processing. *Brain Lang.* **121**, 273–288 (2012).
31. I. Bornkessel-Schlesewsky, M. Schlesewsky, Reconciling time, space and function: A new dorsal-ventral stream model of sentence comprehension. *Brain Lang.* **125**, 60–76 (2013).
32. W. Matchin *et al.*, Agrammatism and paragrammatism: A cortical double dissociation revealed by lesion-symptom mapping. *Neurobiol Lang (Camb)* **1**, 208–225 (2020).
33. W. Matchin, E. Wood, Syntax-sensitive regions of the posterior inferior frontal gyrus and the posterior temporal lobe are differentially recruited by production and perception. *Cereb. Cortex Commun.* **1**, tgaa029 (2020).
34. J. R. Binder, R. H. Desai, The neurobiology of semantic memory. *Trends Cogn. Sci.* **15**, 527–536 (2011).
35. M. A. L. Ralph, E. Jefferies, K. Patterson, T. T. Rogers, The neural and computational bases of semantic cognition. *Nat. Rev. Neurosci.* **18**, 42–55 (2017).
36. A. U. Turken, N. F. Dronkers, The neural architecture of the language comprehension network: Converging evidence from lesion and connectivity analyses. *Front. Syst. Neurosci.* **5**, 1 (2011).
37. H. Axer, C. M. Klingner, A. Prescher, Fiber anatomy of dorsal and ventral language streams. *Brain Lang.* **127**, 192–204 (2013).
38. G. Hickok, D. Poeppel, The cortical organization of speech processing. *Nat. Rev. Neurosci.* **8**, 393–402 (2007).
39. D. López-Barroso *et al.*, Word learning is mediated by the left arcuate fasciculus. *Proc. Natl. Acad. Sci. U.S.A.* **110**, 13168–13173 (2013).
40. C. François *et al.*, Language learning and brain reorganization in a 3.5-year-old child with left perinatal stroke revealed using structural and functional connectivity. *Cortex* **77**, 95–118 (2016).
41. J. Sierpowska *et al.*, White-matter pathways and semantic processing: Intrasurgical and lesion-symptom mapping evidence. *Neuroimage Clin.* **22**, 101704 (2019).
42. N. F. Dronkers, D. P. Wilkins, R. D. Van Valin Jr., B. B. Redfern, J. J. Jaeger, Lesion analysis of the brain areas involved in language comprehension. *Cognition* **92**, 145–177 (2004).
43. J. V. Baldo, A. Arévalo, J. P. Patterson, N. F. Dronkers, Grey and white matter correlates of picture naming: Evidence from a voxel-based lesion analysis of the Boston Naming Test. *Cortex* **49**, 658–667 (2013).
44. I. Bakker-Marshall *et al.*, Theta-band oscillations in the middle temporal gyrus reflect novel word consolidation. *J. Cogn. Neurosci.* **30**, 621–633 (2018).
45. A. Takashima, I. Bakker, J. G. van Hell, G. Janzen, J. M. McQueen, Richness of information about novel words influences how episodic and semantic memory networks interact during lexicalization. *Neuroimage* **84**, 265–278 (2014).
46. A. Takashima, I. Bakker, J. G. van Hell, G. Janzen, J. M. McQueen, Interaction between episodic and semantic memory networks in the acquisition and consolidation of novel spoken words. *Brain Lang.* **167**, 44–60 (2017).
47. D. Perani *et al.*, Neural language networks at birth. *Proc. Natl. Acad. Sci. U.S.A.* **108**, 16056–16061 (2011).
48. J. Brauer, A. Anwander, A. D. Friederici, Neuroanatomical prerequisites for language functions in the maturing brain. *Cereb. Cortex* **21**, 459–466 (2011).
49. A. Giorgio *et al.*, Longitudinal changes in grey and white matter during adolescence. *Neuroimage* **49**, 94–103 (2010).
50. M. L. Berthier, M. A. Lambon Ralph, Dissecting the function of networks underpinning language repetition. *Front. Hum. Neurosci.* **8**, 727 (2014).
51. Parker Jones *et al.*, Sensory-to-motor integration during auditory repetition: A combined fMRI and lesion study. *Front. Hum. Neurosci.* **8**, 24 (2014).
52. J. Sierpowska *et al.*, Words are not enough: Nonword repetition as an indicator of arcuate fasciculus integrity during brain tumor resection. *J. Neurosurg.* **126**, 435–445 (2017).
53. S. Marchina *et al.*, Impairment of speech production predicted by lesion load of the left arcuate fasciculus. *Stroke* **42**, 2251–2256 (2011).

54. N. Janssen *et al.*, A Dissociating the functional roles of arcuate fasciculus subtracts in speech production. *Cereb. Cortex*, in press.
55. G. F. Halwani, P. Loui, T. Rüber, G. Schlaug, Effects of practice and experience on the arcuate fasciculus: Comparing singers, instrumentalists, and non-musicians. *Front. Psychol.* **2**, 156 (2011).
56. J. Fridriksson *et al.*, Impaired speech repetition and left parietal lobe damage. *J. Neurosci.* **30**, 11057–11061 (2010).
57. G. Vallar, A. M. Di Betta, M. C. Silveri, The phonological short-term store-rehearsal system: Patterns of impairment and neural correlates. *Neuropsychologia* **35**, 795–812 (1997).
58. A. Baddeley, Working memory: Looking back and looking forward. *Nat. Rev. Neurosci.* **4**, 829–839 (2003).
59. C. Papagno, Studying cognitive functions by means of direct electrical stimulation: A review. *Neurol. Sci.* **38**, 2079–2087 (2017).
60. F. Leroy *et al.*, New human-specific brain landmark: The depth asymmetry of superior temporal sulcus. *Proc. Natl. Acad. Sci. U.S.A.* **112**, 1208–1213 (2015).
61. G. Herbet, I. Zemmoura, H. Duffau, Functional anatomy of the inferior longitudinal fasciculus: From historical reports to current hypotheses. *Front. Neuroanat.* **12**, 77 (2018).
62. A. D. Friederici, S. M. E. Gierhan, The language network. *Curr. Opin. Neurobiol.* **23**, 250–254 (2013).
63. P. Ripollés *et al.*, Strength of temporal white matter pathways predicts semantic learning. *J. Neurosci.* **37**, 11101–11113 (2017).
64. H. Duffau, P. Gatignol, S. Moritz-Gasser, E. Mandonnet, Is the left uncinate fasciculus essential for language? A cerebral stimulation study. *J. Neurol.* **256**, 382–389 (2009).
65. C. Papagno, Naming and the role of the uncinate fasciculus in language function. *Curr. Neurol. Neurosci. Rep.* **11**, 553–559 (2011).
66. F. Agosta *et al.*, Language networks in semantic dementia. *Brain* **133**, 286–299 (2010).
67. N. Makris *et al.*, Human middle longitudinal fascicle: Segregation and behavioral-clinical implications of two distinct fiber connections linking temporal pole and superior temporal gyrus with the angular gyrus or superior parietal lobule using multi-tensor tractography. *Brain Imaging Behav.* **7**, 335–352 (2013).
68. C. Luo *et al.*, Middle longitudinal fascicle is associated with semantic processing deficits in primary progressive aphasia. *Neuroimage Clin.* **25**, 102115 (2020).
69. G. I. de Zubicaray, S. E. Rose, K. L. McMahon, The structure and connectivity of semantic memory in the healthy older adult brain. *Neuroimage* **54**, 1488–1494 (2011).
70. S. Sarubbo *et al.*, Uncovering the inferior fronto-occipital fascicle and its topological organization in non-human primates: The missing connection for language evolution. *Brain Struct. Funct.* **224**, 1553–1567 (2019).
71. R. B. Mars *et al.*, Concurrent analysis of white matter bundles and grey matter networks in the chimpanzee. *Brain Struct. Funct.* **224**, 1021–1033 (2019).
72. A. G. Ramayya, M. F. Glasser, J. K. Rilling, A DTI investigation of neural substrates supporting tool use. *Cereb. Cortex* **20**, 507–516 (2010).
73. D. Stout, N. Toth, K. Schick, T. Chaminade, Neural correlates of Early Stone Age toolmaking: Technology, language and cognition in human evolution. *Philos. Trans. R. Soc. Lond. B Biol. Sci.* **363**, 1939–1949 (2008).
74. A. Faisal, D. Stout, J. Apel, B. Bradley, The manipulative complexity of Lower Paleolithic stone toolmaking. *PLoS One* **5**, e13718 (2010).
75. L. L. Chao, J. V. Haxby, A. Martin, Attribute-based neural substrates in temporal cortex for perceiving and knowing about objects. *Nat. Neurosci.* **2**, 913–919 (1999).
76. A. Martin, C. L. Wiggs, L. G. Ungerleider, J. V. Haxby, Neural correlates of category-specific knowledge. *Nature* **379**, 649–652 (1996).
77. K. L. Bryant, T. M. Preuss, "A comparative perspective on the human temporal lobe" in *Digital Endocasts*, E. Bruner, N. Ogihara, H. C. Tanabe, Eds. (Springer Japan, Tokyo, Japan, 2018), pp. 239–258.
78. S. Vickery *et al.*, Chimpanzee brain morphometry utilizing standardized MRI preprocessing and macroanatomical annotations. *eLife* **9**, e60136 (2020).
79. D. Falk *et al.*, Identification of in vivo sulci on the external surface of eight adult chimpanzee brains: Implications for interpreting early hominin endocasts. *Brain Behav Evol* **91**, 45–58 (2018).
80. F. M. Krienen, R. L. Buckner, "Human association cortex: Expanded, untethered, neotenous, and plastic" in *Evolutionary Neuroscience*, J. H. Kaas, Ed. (Academic Press, ed. 2, 2020), chap. 35, pp. 845–860.
81. R. Mars, R. E. Passingham, F. X. Neubert, L. Verhagen, J. Sallet, "Evolutionary specializations of human association cortex" in *Evolution of Nervous Systems*, J. H. Kaas, Ed. (Academic Press, ed. 2, 2016), pp. 185–205.
82. J. P. Marques *et al.*, MP2RAGE, a self bias-field corrected sequence for improved segmentation and T1-mapping at high field. *Neuroimage* **49**, 1271–1281 (2010).
83. M. P. Zwiers, Patching cardiac and head motion artefacts in diffusion-weighted images. *Neuroimage* **53**, 565–575 (2010).
84. T. E. J. Behrens *et al.*, Characterization and propagation of uncertainty in diffusion-weighted MR imaging. *Magn. Reson. Med.* **50**, 1077–1088 (2003).
85. J. L. R. Andersson, S. Skare, J. Ashburner, How to correct susceptibility distortions in spin-echo echo-planar images: Application to diffusion tensor imaging. *Neuroimage* **20**, 870–888 (2003).
86. M. F. Glasser *et al.*, *Improved Cortical Myelin Maps in Humans, Chimpanzees, and Macaques Allow Identification of Putative Areal Homologies* (Society for Neuroscience, New Orleans, LA, 2012).
87. M. F. Glasser, D. C. Van Essen, Mapping human cortical areas in vivo based on myelin content as revealed by T1- and T2-weighted MRI. *J. Neurosci.* **31**, 11597–11616 (2011).
88. S. M. Smith *et al.*, Advances in functional and structural MR image analysis and implementation as FSL. *Neuroimage* **23** (suppl. 1), S208–S219 (2004).
89. S. M. Smith, Fast robust automated brain extraction. *Hum. Brain Mapp.* **17**, 143–155 (2002).
90. M. S. Graham, I. Drobnjak, H. Zhang, Realistic simulation of artefacts in diffusion MRI for validating post-processing correction techniques. *Neuroimage* **125**, 1079–1094 (2016).
91. T. E. J. Behrens, H. J. Berg, S. Jbabdi, M. F. S. Rushworth, M. W. Woolrich, Probabilistic diffusion tractography with multiple fibre orientations: What can we gain? *Neuroimage* **34**, 144–155 (2007).
92. M. F. Glasser *et al.*; WU-Minn HCP Consortium, The minimal preprocessing pipelines for the Human Connectome Project. *Neuroimage* **80**, 105–124 (2013).
93. L. Li *et al.*, Chimpanzee (*Pan troglodytes*) precentral corticospinal system asymmetry and handedness: A diffusion magnetic resonance imaging study. *PLoS One* **5**, e12886 (2010).
94. C. J. Donahue, M. F. Glasser, T. M. Preuss, J. K. Rilling, D. C. Van Essen, Quantitative assessment of prefrontal cortex in humans relative to nonhuman primates. *Proc. Natl. Acad. Sci. U.S.A.* **115**, E5183–E5192 (2018).
95. H. Wickham, tidyverse: Easily Install and Load the 'Tidyverse'. R Package Version 1.2.1 (2017). https://cran.r-project.org/web/packages/tidyverse/index.html. Accessed 6 June 2022.
96. D. Robinson *et al.*, broom: Convert Statistical Analysis Objects into Tidy Tibbles. R Package Version 0.5.2 (2019). https://cran.r-project.org/web/packages/broom/index.html. Accessed 6 June 2022.
97. L. Henry, H. Wickham, purrr: Functional Programming Tools. R Package Version 0.3.2 (2019). https://cran.r-project.org/web/packages/purrr/index.html. Accessed 6 June 2022.
98. C. J. Donahue *et al.*, Using diffusion tractography to predict cortical connection strength and distance: A quantitative comparison with tracers in the monkey. *J. Neurosci.* **36**, 6758–6770 (2016).
99. H. Azadbakht *et al.*, Validation of high-resolution tractography against in vivo tracing in the macaque visual cortex. *Cereb. Cortex* **25**, 4299–4309 (2015).
100. M. P. van den Heuvel *et al.*, Comparison of diffusion tractography and tract-tracing measures of connectivity strength in rhesus macaque connectome. *Hum. Brain Mapp.* **36**, 3064–3075 (2015).
101. J. I. Berman, M. R. Lanza, L. Blaskey, J. C. Edgar, T. P. L. Roberts, High angular resolution diffusion imaging probabilistic tractography of the auditory radiation. *AJNR Am. J. Neuroradiol.* **34**, 1573–1578 (2013).
102. E. E. Hecht, D. A. Gutman, B. A. Bradley, T. M. Preuss, D. Stout, Virtual dissection and comparative connectivity of the superior longitudinal fasciculus in chimpanzees and humans. *Neuroimage* **108**, 124–137 (2015).
103. K. H. Maier-Hein *et al.*, The challenge of mapping the human connectome based on diffusion tractography. *Nat. Commun.* **8**, 1349 (2017).
104. C. Reveley *et al.*, Superficial white matter fiber systems impede detection of long-range cortical connections in diffusion MR tractography. *Proc. Natl. Acad. Sci. U.S.A.* **112**, E2820–E2828 (2015).
105. R. B. Mars, S. Jbabdi, M. F. S. Rushworth, A common space approach to comparative neuroscience. *Annu. Rev. Neurosci.* **44**, 69–86 (2021).
106. J. Sierpowska *et al.*, Comparing human and chimpanzee temporal lobe neuroanatomy reveals modifications to human language hubs beyond the frontotemporal arcuate fasciculus. Donders Repository. https://doi.org/10.34973/warf-df84. Deposited 7 June 2022.